December 2005 Volume 5 • Number 12

www.aspbs.com/jnn

Journal of NANOSCIENCE and NANOTECHNOLOGY

Editor-in-Chief: Hari Singh Nalwa, USA

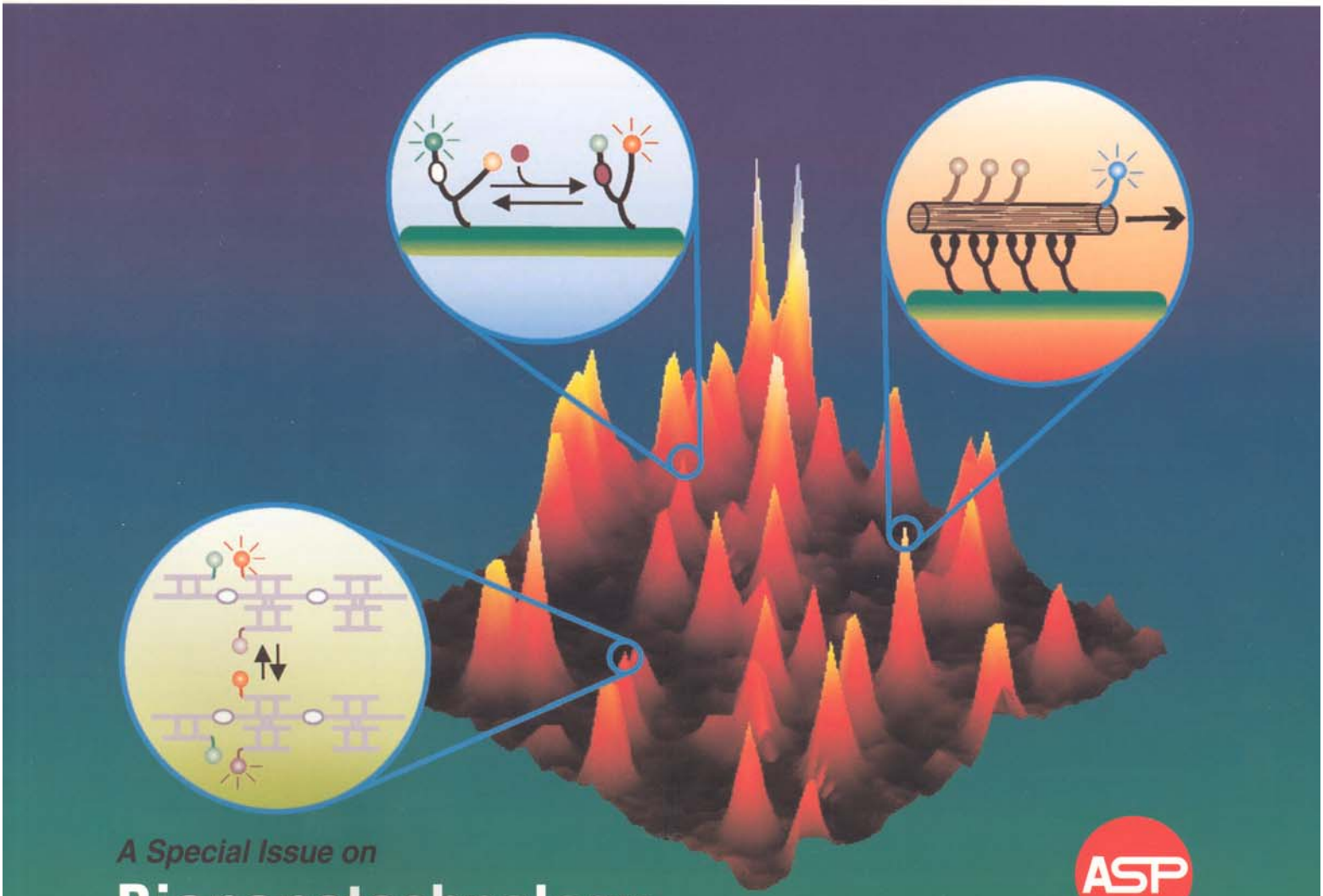

A Special Issue on

Bionanotechnology

GUEST EDITOR: Peixuan Guo

ASP

Journal of
Nanoscience and Nanotechnology
Vol. 5, 1–11, 2005

REVIEW

Single Molecule Fluorescence Control for Nanotechnology

David Rueda and Nils G. Walter*

Department of Chemistry,University of Michigan,
930 N. University Avenue, Ann Arbor, Michigan 48109-1055, USA

Nanoscience and nanotechnology are providing fresh approaches to engineer materials with practical applications such as molecular-sized therapeutic and diagnostic devices, drug delivery vehicles, environmental sensors, high-rate manufacturing platforms, and self-assembling nanomachines. In many cases, researchers are mimicking biological systems that easily achieve molecular scale control through directed self-assembly. In parallel, a revolution has occurred in the basic sciences, which utilizes recent advances in fluorescence microscopy to achieve single molecule detection capability. The future will see a merger of these two separate research thrusts, as single molecule detection will afford optimal control over the assembly and performance of individual nanoscale devices.

Keywords: Conformational Change, Fluorescence Microscopy, Fluorescence Resonance Energy Transfer, FRET, Nucleic Acid Nanoscience.

CONTENTS

1. INTRODUCTION

Nanoscience and nanotechnology are providing fresh approaches to engineer materials with practical applications such as molecular-sized therapeutic and diagnostic devices, drug delivery vehicles, environmental sensors, high-rate manufacturing platforms, and self-assembling nanomachines. Over billions of years of evolution, nature has perfected the use of nanometer-scale biopolymers as building blocks for the self-assembly of the structural and functional components of cells. For example, proteins and nucleic acids self-assemble to create nanoscale molecular complexes, such as the replication, transcription, and translation machineries, which are examples of energy consuming, directed molecular motors with useful properties for nanotechnology applications. Consequently, there has been a substantial effort in nanotechnology to mimic nature's ability to build functional nanostructures using the same raw materials.[1, 2]

An important challenge in nanotechnology is to control the assembly and performance of nanoscale objects. Fluorescence resonance energy transfer (FRET) between a donor and an acceptor fluorophore, site-specifically attached to a biopolymer, was recognized early on as a powerful molecular ruler in the 2–10 nanometer distance range.[3, 4] For a given donor–acceptor fluorophore pair where the donor emission spectrum sufficiently overlaps with the acceptor excitation spectrum and both tumble isotropically at the end of their attachment linkers, the energy transfer efficiency primarily depends on the inverse sixth power of the distance between the two fluorophores. This strong distance dependence of FRET, together with the fact that it fills the vital gap between the distance sensitivities of other techniques such as NMR spectroscopy (<1 nm) and electron microscopy (>10 nm), makes it such an attractive tool to measure biomolecular distances.[5, 6]

*Author to whom correspondence should be addressed.

REVIEW

Recent advances in fluorescence microscopy[7] have allowed us to achieve single molecule FRET (sometimes referred to as single pair FRET) detection of the molecular motions of individual biopolymers and their complexes at the nanoscale.[8–13] Such a single molecule approach has two major advantages over bulk solution (ensemble) measurements. First, it reveals the stochastic fluctuations of biomolecules between distinct conformational states, with the ability to measure all fluctuation rate constants in a single experiment even under equilibrium conditions. Second, transient intermediates and parallel reaction pathways including static and dynamic heterogeneities, which are often difficult or impossible to detect in ensemble-averaged measurements, can be directly observed in single molecule experiments. Therefore single molecule fluorescence, and particularly FRET microscopy, has the unique potential to achieve real-time control over the assembly and performance of individual nanoscale devices. We are just beginning to live up to this potential.

The present review summarizes recent advances in single molecule FRET microscopy and nucleic acid nanotechnology and then suggests to synergistically merge the two fields. In Section 2, we describe two major techniques that achieve single molecule sensitivity, confocal and total internal reflection (TIR) fluorescence microscopy. In Section 3, we focus on two landmark examples that illustrate how single molecule FRET microscopy has been applied to dissect the structural dynamics of nucleic acid enzymes that are essential for the processing of genetic information, the hairpin ribozyme and the ribosome.[14–17] In Section 4, we illustrate the application of nucleic acids in nanotechnology by describing some of the pioneering work by Seeman and co-workers on building DNA based nanomechanical devices.[18, 19] In Section 5, we outline our vision for applying single molecule fluorescence detection to nucleic acid nanotechnology as a tool to monitor individual nanodevices at work and to characterize their structural and functional performance. Naturally, such a review cannot do justice to all the stunning advances in the fields of single molecule fluorescence microscopy and nucleic acid nanotechnology so that we would like to refer the interested reader to some more comprehensive reviews for further inspiration.[7–10, 12, 13, 20, 21]

2. ACHIEVING SINGLE MOLECULE FLUORESCENCE SENSITIVITY

For over a decade now, we have witnessed extraordinary technological advances caused by the development of ultrasensitive optical tools that enable single molecule

David Rueda is currently a Research Fellow in the laboratory of Prof. Nils Walter at the University of Michigan (Department of Chemistry), Ann Arbor. He graduated in 1997 with a degree in chemical engineering from the Swiss Institute of Technology in Lausanne (Switzerland), specialized in Physical Chemistry. For his Diploma Thesis research, he studied the non-linear intensity dependence in the infrared multiphoton excitation and dissociation of methanol pre-excited to different energies in the laboratory of Prof. Martin Quack at the Swiss Institute of Technology in Zürich (Switzerland). In 2001, he obtained his Ph.D. under the supervision of Prof. Thomas R. Rizzo back in Lausanne, where he characterized the vibrational dependence of the torsional potential of jet-cooled methanol. Since then, he has been studying the correlation between the structure, function and dynamics in small RNA enzymes using fluorescence resonance energy transfer and single molecule microscopy. His current research interests lie in the study of the structural dynamics and function of RNA and RNA-protein complexes. Dr. Rueda has been awarded the Ciba Specialty Chemical Award for the best Diploma thesis (1997) and a Postdoctoral Research Fellowship from the Swiss National Funds (2001).

Nils Walter is an Associate Professor of Chemistry at the University of Michigan, Ann Arbor. He graduated from the Technical University of Darmstadt, Germany, with a Diploma in Chemistry in 1991 and received his thesis degree in 1995 at the Max-Planck-Institute for Biophysical Chemistry in Göttingen, Germany, with Nobel Laureate Manfred Eigen. He moved to the US to work as a postdoctoral fellow with John Burke at the University of Vermont on small catalytic RNAs before taking a faculty position at Michigan in 1999. Dr. Walter is a winner of the Camille Dreyfus Teacher-Scholar Award (2004), the Dow Corning Assistant Professorship (2002), the 1995 Otto-Hahn Medal for Outstanding Researchers of the Max-Planck Society, a Postdoctoral Research Fellowship from the Alexander von Humboldt Foundation and a Kekulé Pre-doctoral Scholarship from the Fonds of the German Chemical Industry Association. He has about fifty publications, including several chapters in books. Over the past ten years, Dr. Walter's studies have focused on the structural dynamics that lead to catalysis in RNA enzymes (ribozymes), as related to gene therapy applications against human diseases. Single-molecule RNA enzymology, the use of ribozymes as nanoscale biosensors, and the fluorescence imaging of nanotechnological devices are topics where Dr. Walter has shifted his focus most recently.

detection in aqueous samples.[7] These tools have led to observations of individual molecules as they undergo biological reactions. While complementary to more traditional ensemble measurements, single molecule techniques have proven to offer numerous advantages:[9, 13] (i) Single molecule detection uncovers the properties of individual molecules that would otherwise be hidden in the ensemble average. For example, statically or dynamically heterogeneous subpopulations are resolved and rare and/or transient reaction intermediates are detected (where static heterogeneity describes kinetically distinct subpopulations that do not significantly interconvert, while dynamic heterogeneity implies that they do). (ii) Monitoring reactions one molecule at a time eliminates the requirement that all observed molecules be synchronized to derive quantitative kinetic information. (iii) Single molecule detection allows one to follow a specific molecule for an extended period of time.

One of the most fruitful applications of single molecule detection has resulted from its combination with FRET. FRET arises from the interaction of the electronic transition dipole moments of a donor fluorophore and a spectrally matched acceptor fluorophore.[3–6,22] Following excitation of the donor, energy is transferred to the acceptor and, thus, the fluorescence emission of the acceptor increases, while the donor's emission decreases simultaneously. The efficiency of this process, E_{FRET}, is given by:

$$E_{\mathrm{FRET}} = \frac{1}{1+\left(\frac{R}{R_0}\right)^6} \tag{1}$$

where R is the distance between the two fluorophores, and R_0 is the Förster distance, or distance at which 50% efficiency is observed. R_0, typically in the range of 3–8 nm, depends on the spectral overlap of the fluorescence emission spectrum of the donor and the fluorescence excitation spectrum of the acceptor, as well as their relative orientation. The strong inverse sixth power dependence of the FRET efficiency on the fluorophore distance makes it a very effective spectroscopic ruler to measure distances in the 2–10 nm range.[3–6, 22] Depending on how the fluorophores are incorporated into the system under study, FRET can provide for a measure of inter- or intramolecular distances. Distance changes in a single molecule (or particle) that are observed along its reaction pathway in real-time monitor a reaction coordinate that offers a view of conformational intermediates and their structural dynamics. Thus, single molecule FRET (smFRET) offers the opportunity to directly access the structural fluctuations of biopolymers and their complexes, examine their folding and unfolding kinetics and thermodynamics, and correlate structural changes with, for example, enzymatic events.[9, 13]

One of the most important criteria to achieve single molecule detection is to virtually eliminate background fluorescence. Typical sources of background fluorescence are an excess of free fluorophore in solution, autofluorescence

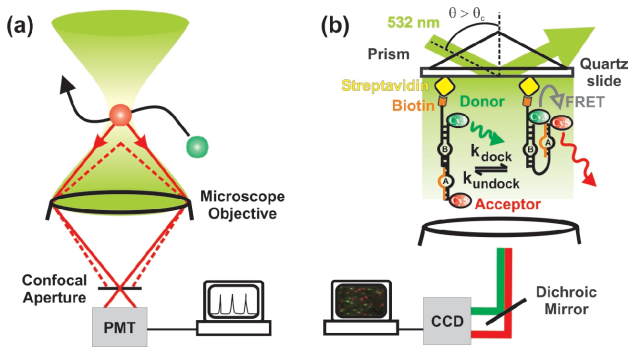

Fig. 1. Principles of single molecule detection: confocal fluorescence microscopy (a) and total internal reflection fluorescence microscopy (b). See text for details.

from the sample, and luminescence from the optical and substrate surfaces. Two major experimental techniques are commonly used to reduce these background signals, essentially by limiting the detection volume: Confocal and TIR fluorescence microscopy (Fig. 1). The basic principle of confocal fluorescence microscopy is depicted in Figure 1a.[23] Here, a laser beam is focused to a spot to illuminate the sample. A small aperture positioned in the image plane suppresses background signal by greatly reducing the transmission of out-of-focus light to the detector. When a fluorescent molecule diffuses through the focal volume, it becomes excited and fluoresces. The in-focus emission (solid red lines, Fig. 1a) focuses back through the image plane and reaches the detector (typically a photomultiplier tube, PMT, or avalanche photodiode, APD), whereas the emission from out-of-focus areas (dashed red lines, Fig. 1a) does not focus in the image plane, and thus does not pass through the pinhole. As a result, only the sample in a small (femtoliter) effective confocal volume element is observed with increased contrast (better signal-to-noise) and reduced diffuse, out-of-focal-plane background. Recordings of fluorescence intensity over time (henceforth referred to as "time trajectories") from confocal microscopy consist of sudden bursts of intensity caused by fluorescent molecules diffusing through the detection volume. smFRET time trajectories can be obtained by splitting the fluorescence image with an appropriate dichroic mirror after the confocal aperture and using a second detector to measure the acceptor's fluorescence signal. Relative smFRET efficiencies, E, are then calculated as:

$$E = \frac{I_A}{(I_{\mathrm{A}} + \gamma I_{\mathrm{D}})} \tag{2}$$

where I_{A} and I_{D} are the acceptor and donor emission intensities, respectively, and γ is the acceptor-to-donor ratio of the products of fluorescence quantum yield and the instrument detection efficiency in the respective channel (typically $\gamma \approx 1$).[24] The fluorescence burst durations obtained from confocal microscopy provide a measurement of the diffusion time of a fluorophore labeled molecule through

REVIEW

the focal volume element. This measure can be used to monitor biological reactions during which the molecule (or complex) undergoes size changes that affect its diffusion coefficient.

One of the major limitations of confocal microscopy arises from the short observation window, which is determined by the diffusion time of the fluorescent molecule through the laser excitation volume. However, this limitation can be overcome by immobilizing the sample in an agarose gel,[25] or through the specific interaction of a biotinylated target molecule with surface-bound streptavidin,[26] followed by scanning the confocal volume over the sample in a raster pattern. Additional disadvantages of confocal microscopy are the low throughput of light through the confocal aperture, and the fact that the excitation light illuminates the entire depth of the sample, thus causing photobleaching in areas where data are not being taken. Multiphoton confocal microscopy is a variation that permits to decrease the amount of out-of-focus photobleaching and further increase spatial resolution.[27]

As an alternative to confocal microscopy, TIR fluorescence microscopy reduces the excitation volume to a thin sheet at the interface between a microscope slide and a solution (Fig. 1b).[28] A laser beam reaches the slide through a prism (or the objective) at an angle of incidence (θ) that is larger than the critical angle (θ_c), beyond which the refracted beam does not fully penetrate the solution. The critical angle is determined by Snell's law as:

$$\sin\theta_c = \frac{n_s}{n_w} \tag{3}$$

where n_s and n_w are the indices of refraction of the slide and the aqueous solution, respectively. However, the wave properties of the incident light result in an evanescent field at the interface, whose intensity, $I(z)$, decays exponentially into the solution:[28]

$$I(z) = I_0 \exp\left(\frac{-z}{d}\right)$$
$$d = \frac{\lambda_0}{4\pi}(n_s^2 \sin^2\theta - n_w^2)^{-1/2}, \quad (\theta > \theta_c) \tag{4}$$

where z is the distance from the slide surface into the solution, d is the evanescent field penetration depth, and λ_0 is the excitation light wavelength in vacuum. Typically, the angle of incidence is only a few degrees above the critical angle, and the resulting penetration depth is ~100 nm. Consequently, sample molecules farther away from the slide surface are not exposed to excitation light and do not give rise to a background signal. This selectivity makes TIR a useful technique to study distributions, motions, or kinetics of fluorescent molecules at a slide surface in the presence of possibly much higher concentrations of fluorophores in the bulk solution. In the example in Figure 1b, a fluorophore labeled hairpin ribozyme has been immobilized at the slide/water interface using a biotin/streptavidin interaction. This hairpin ribozyme is in equilibrium between an extended and a compact folded conformation. In the extended conformation, the donor fluorophore (Cy3) is excited by the evanescent field, and its fluorescence is collected through the microscope objective onto an area detector (an intensified CCD camera). When the hairpin ribozyme folds into the compact conformation, the acceptor fluorophore is excited by FRET, and the CCD camera detects its emission. The emissions of the donor and the acceptor are separated with appropriate dichroic optics, and detected as two side-by-side images on the CCD chip. A pseudo-colored overlay of the two images is shown in Figure 1b, where ribozyme molecules in the extended conformation appear as green spots, and those in the folded conformation appear as red spots. A time trajectory of relative smFRET efficiency (as shown in Fig. 2b) can be calculated from integration of individual donor and acceptor spot intensities and using Eq. (2).

TIR fluorescence microscopy overcomes some of the disadvantages of confocal microscopy. Limiting the excitation to a small sheet volume at the slide/solution interface decreases the background signal as well as the amount of photobleaching outside the observation volume. Furthermore, TIR illumination and imaging with a CCD camera readily enable the observation of a wide field of single molecules without scanning the sample so that multiple molecules can be detected in parallel, even if they are moving, thus decreasing the time necessary to collect a statistically significant number of single molecule time traces. However, the time resolution with current CCD technology

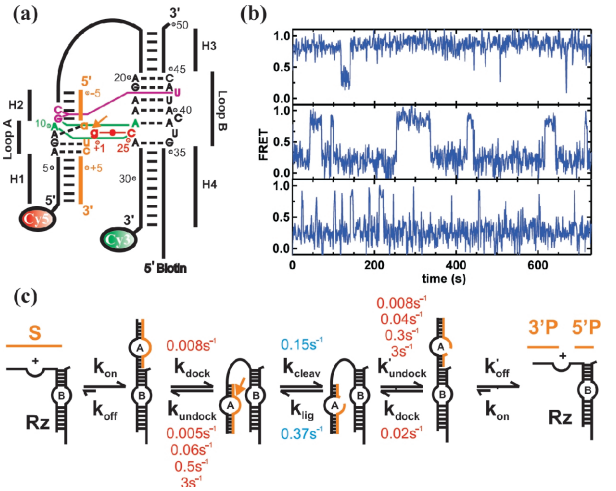

Fig. 2. Single molecule enzymology of the hairpin ribozyme.[15, 51] (a) Secondary structure of the hairpin ribozyme. (b) Single molecule FRET time trajectories of three individual molecules that belong to distinct subpopulations. The differences in folding dynamics are apparent from the dwell times in the docked (high FRET) state. (c) Minimal reaction pathway of the hairpin ribozyme with rate constants derived from single molecule fluorescence imaging. Reprinted with permission from [15], X.Zhuang et al., *Science* 296, 1473 **(2002)** and [51], D. Rueda et al., *Proc. Natl. Acad. Sci. USA* 101, 10066 **(2004)**.

is still ~100-fold lower than with the fastest APDs used in confocal fluorescence microscopy.

3. CAPABILITIES OF SINGLE MOLECULE FLUORESCENCE MICROSCOPY

In the past few years, confocal and TIR fluorescence microscopy have both been applied extensively to studies of structure-function relationships in biopolymers (for review see Refs. [7–10, 12, 13]). To showcase the capabilities of single molecule fluorescence microscopy, we describe in the following two exemplary applications that illustrate how smFRET using TIR excitation has been exploited to gain important fundamental insights into RNA structural dynamics and how they lead to biological function.

3.1. Folding Dynamics and Function of Single Hairpin Ribozymes

The versatile functionalities of RNA are beginning to be exploited as basis for novel reverse genetics and therapeutic agents,[29–32] components of biosensors,[33, 34] and components of nanoscale fabrics.[35] In nature, RNA plays important enzymatic roles in numerous cellular processes such as gene expression,[36] splicing,[37, 38] and translation.[39, 40] In the rolling-circle replication of viral satellite RNAs, for example, RNA enzymes (ribozymes) play a critical role by processing multimeric intermediates into genome-length circles.[41, 42] Four different such ribozymes occur naturally, the hairpin, the hammerhead, the hepatitis delta virus, and the *Neurospora* VS ribozyme. Despite their differences in size, structure, and residues involved in catalysis, all four ribozymes catalyze the same, site-specific and reversible internal backbone cleavage reaction, which generates 2′,3′-cyclic phosphate and 5′-hydroxyl termini in their products. Due to their small size (~40–160 nucleotides) they are grouped as the class of "small ribozymes." The hairpin ribozyme is found in a group of plant pathogens, including the tobacco ring spot virus satellite RNA.[41, 43] In its natural form, the hairpin ribozyme is part of a four-way junction, which has been engineered into a minimal, fully active form consisting of two helix-loop-helix domains, A and B, as shown in Figure 2a.[6]

In the active conformation, the two loops dock together, forming tertiary contacts that stabilize a compact fold (Fig. 2a).[44] This docking event is associated with an induced fit resulting in a dramatic rearrangement of secondary structure, as evident from the fact that the NMR structures of loops A and B alone[45, 46] differ substantially from the crystal structure of the docked complex.[44, 47] The three main tertiary docking interactions between domains A and B are: (i) The G + 1 binding pocket, where G + 1 in domain A forms a base pair with C25 in domain B (Fig. 2a, red); (ii) the ribose zipper, a network of hydrogen bonds connecting A10 and G11 in domain A with A24 and C25 in domain B (Fig. 2a, green); and (iii) the U42 binding pocket, where U42 forms hydrogen bonds with G11 and C12 in domain A and with A22 and A23 in domain B (Fig. 2a, purple).

A number of studies have elucidated the five, fully reversible, sequential steps on the reaction pathway of the hairpin ribozyme (Fig. 2c).[6] First, the substrate binds to the ribozyme, forming the secondary structure of domain A in an initially extended (undocked) and still inactive ribozyme-substrate complex. Second, domains A and B dock, forming the tertiary structure of the compact, catalytically active conformer (Fig. 2a). Third, the ribozyme cleaves the substrate. Fourth, the product complex undocks. Finally, the undocked product complex releases the 5′ and 3′ products by dissociation. The hairpin ribozyme is an ideal model system to study the relationship between RNA folding and catalysis, as its catalytic function provides a direct readout for native docking interactions and its small size enables convenient chemical synthesis including the attachment of fluorophores and biotin for smFRET experiments by prism based TIR illumination (Fig. 1b).

SmFRET experiments by Walter, Chu, and co-workers first demonstrated a strong correlation between the structural dynamics and catalytic function of the hairpin ribozyme.[15] A domain-terminal donor/acceptor fluorophore pair was found to exhibit anticorrelated fluorescence signals that correspond to conformational changes between the extended and docked conformers. The resulting relative FRET efficiencies in the extended and folded conformations are ~0.2 and ~0.8, respectively (Fig. 2b). Importantly, the distributions of dwell times in the extended (low FRET) and docked (high FRET) states give access to the docking and undocking rate constants, respectively.[15, 48] One of the initial concerns of course was the introduction of artifacts by the necessary surface immobilization. The cleavage kinetics of single immobilized molecules was therefore measured and found to coincide with that in bulk solution, demonstrating that surface effects are in fact negligible.[15] Indeed, all RNA systems studied to date have not exhibited detectable interactions with glass surfaces that are negatively charged at neutral or basic pH.[13] Systems involving proteins, by contrast, require surface passivation through reagents such as polyethylene glycol to avoid denaturation.[49, 50]

Surprisingly, the hairpin ribozyme exhibits complex folding dynamics with (at least) four subpopulations of distinct undocking kinetics that were clearly distinguished by smFRET (Fig. 2b). (To ensure that the docking and undocking kinetics was measured unperturbed by catalysis, a non-cleavable substrate analogue with a 2′-O-methyl modification at the cleavage site was used in all of the following studies.) Moreover, throughout an smFRET time trajectory, molecules maintain similar dwell times in the docked state, revealing a pronounced memory

effect (Fig. 2b). In fact, after 3 hours less than 5% of all time trajectories show any interconversion between subpopulations.[15] Additional measurements using saturating concentrations of the reaction products (rendered nonreactive by introduction of a 3′-phosphate[15]) showed that the ribozyme-product complex likewise exhibits (at least) four undocking rate constants and a strong memory effect. Kinetic simulations revealed that these complex structural dynamics quantitatively explain the heterogeneous cleavage kinetics of the hairpin ribozyme, which it shares with many catalytic RNAs. These observations led us to conclude that a strong coupling between structural dynamics and function is a general phenomenon in RNA.[15] More recent experiments using a combination of smFRET, cleavage and ligation assays, and matrix-algebra assisted kinetic simulations have allowed us to derive rate constants for the reversible cleavage (chemistry) step and so fully dissect the kinetic steps on the hairpin ribozyme's reaction pathway (Fig. 2c).[51] Using this approach, we were able to quantify the effects of site-specific chemical modifications on the rate constants of folding and chemistry. Interestingly, we found that modifications far removed from the site of catalysis can impact the rate constants of both folding and chemistry. This discovery led us to propose that a network of coupled molecular motions connects distant parts of the molecule with its reaction site, as previously suggested for proteins.[51,52] Intriguingly, the observed molecular heterogeneity with memory effect persists under all buffer conditions and for all modifications tested so far.

Measuring the rates of docking and undocking of the hairpin ribozyme also has allowed us to characterize the transition state for this elementary folding reaction and its key determinants, by using a combination of smFRET, site-specific mutations, metal ion titrations, and electrostatic calculations.[14] Specifically, the transition state free energy relative to that of the docked state is calculated from the measured docking rate constant as:

$$\Delta G^{\mp}_{\mathrm{dock}} = -RT \ln k_{\mathrm{dock}} \qquad (5)$$

The transition state free energy relative to that of the undocked state is calculated similarly from the undocking rate constant. Disruption of a tertiary contact by a site-specific mutation results in changes, termed $\Delta\Delta G^{\mp}_{\mathrm{dock}}$ and $\Delta\Delta G^{\mp}_{\mathrm{undock}}$, of the docking and undocking transition state free energies, respectively, of the mutant relative to those of the wild-type (Fig. 3b). A coefficient, Φ, can then be defined as:

$$\Phi = \frac{\Delta\Delta G^{\mp}_{\mathrm{dock}}}{(\Delta\Delta G^{\mp}_{\mathrm{dock}} - \Delta\Delta G^{\mp}_{\mathrm{undock}})} \qquad (6)$$

that indicates whether the tertiary contact disrupted by the mutation is already formed in the transition state ($\Phi \approx 1$; late transition state; mutational effect mostly on docking) or not ($\Phi \approx 0$; early transition state; mutational

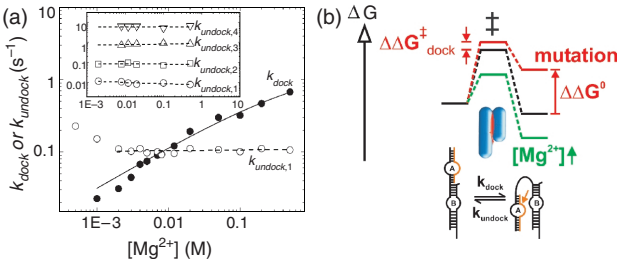

Fig. 3. The folding transition state of the hairpin ribozyme from single molecule analysis.[14] (a) Effect of metal ions on the rate constants for docking and undocking of the hairpin ribozyme at 37 °C. Inset: Dependence of the undocking rate constants of the four subpopulations observable at 25 °C. (b) Free energy diagram of the docking and undocking folding transition. Mutations disrupting a tertiary contact (red) were found to specifically destabilize the docked state, while increases in Mg^{2+} concentration (green) stabilize the transition and docked states to a similar extent. These observations lead to a model of the docking transitions state where the two domains (blue cylinders) are in near-contact and are stabilized by a high concentration of diffusely bound Mg^{2+} ions at their interface (red). Reproduced with permission from [14], G. Bokinsky et al., *Proc. Natl. Acad. Sci. USA* 100, 9302 (**2003**).

effect mostly on undocking).[53] Small fractional Φ values (i.e., mutational effects mostly on undocking) were obtained for mutations that disrupt specifically one of the hydrogen bonds involved in the G+1 binding pocket, the ribose zipper, or the U42 binding pocket, suggesting that these bonds are at most partially formed in the transition state.[14] By contrast, the rate of docking increases >40-fold when raising the Mg^{2+} concentration from 1 to 500 mM, while the rate of undocking remains largely constant (Fig. 3a), indicating that Mg^{2+} interactions are already fully established in the transition state (i.e., Mg^{2+} is taken up upon transit from the undocked to the transition state, and remains bound in the docked state). Figure 3b summarizes the resulting free energy profile for the docking transition of the hairpin ribozyme. Electrostatic modeling shows that the most plausible interpretation for these data is that, in the transition state, domains A and B are in a close-to-contact configuration not very different from that of the docked state (Fig. 3b), even though the native tertiary contacts are at most partially formed.[14]

The experiments described above clearly demonstrate that single molecule fluorescence imaging provides detailed quantitative information on the structural dynamics of individual nucleic acid molecules capable of adopting two (or more) conformations and gives access to distinct subpopulations that otherwise would be ensemble-averaged.

3.2. tRNA Dynamics on Single Ribosomes

The prokaryotic ribosome is a ribonucleoprotein complex composed of over 50 proteins and a small and two large RNAs that are organized into the 30S and 50S subunits (Fig. 4a).[39,40] The ribosome orchestrates and catalyzes protein synthesis in all living organisms following instructions encoded in messenger RNA (mRNA). Three sequential mRNA bases form a codon that determines which amino

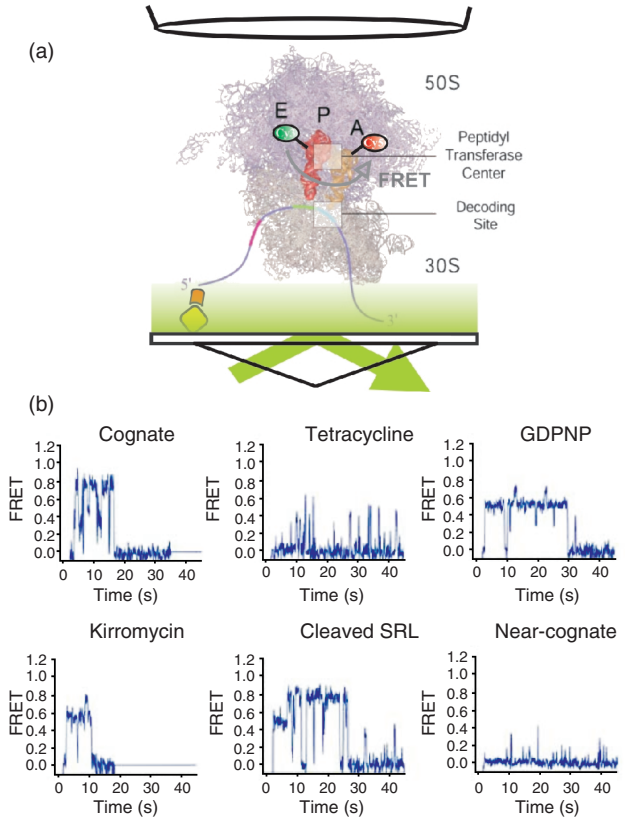

Fig. 4. tRNA dynamics on single ribosomes.[16, 17] (a) Experimental scheme for tethering and fluorescently detecting single ribosomes. Single ribosomes bound to a 5′-biotinylated mRNA are immobilized on a glass surface by binding to the protein streptavidin. A Cy3-labeled tRNA is initially loaded onto the P site. A Cy5-labeled tRNA is then accommodated onto the A site, giving rise to a specific FRET signal. (b) Resulting single molecule FRET time trajectories that monitor tRNA dynamics during selection and incorporation in the absence ("Cognate") and presence of various inhibitors. See text for details. Reproduced with permission from [16], S. C. Blanchard et al., *Nat. Struct. Mol. Biol.* 11, 1008 **(2004)**.

acid will be incorporated during each elongation step by guiding the selection of a specific aminoacyl-tRNA (aa-tRNA) on the ribosome. There are three aa-tRNA binding sites on the ribosome (A, P, and E sites, Fig. 4a). A single cycle by the ribosome can be summarized as follows:[16, 54, 55] (i) An aa-tRNA forms a ternary complex with protein elongation factor Tu (EF-Tu) and GTP. (ii) The ternary complex binds to the 50S subunit through protein–protein interactions with L7/L12. (iii) The aa-tRNA anticodon base pairs to the mRNA codon at the A site within the 30S subunit. (iv) Correct codon recognition by the decoding site (Fig. 4a) triggers GTP hydrolysis by EF-Tu. A non-cognate aa-tRNA will be rejected at this stage. (v) Release of inorganic phosphate induces a conformational change in EF-Tu, leading to factor dissociation and accommodation of the 3′ end of the aa-tRNA in the peptidyl transferase center (PTC, Fig. 4a) within the 50S subunit. (vi) A peptide bond is formed by peptidyl transfer from the tRNA in the P site to the aa-tRNA in the A site. (vii) Translocation of the mRNA:tRNA complex resets the ribosome for the next round of elongation. Ribosomes are capable of incorporating 5–20 amino acids per second in this fashion, with as few as five errors per thousand, on average.[56]

Single molecule fluorescence studies of immobilized bacterial (*Escherichia coli*) ribosomes were first conducted by Hochstrasser and coworkers.[57] More recently, Chu, Puglisi, and coworkers have used TIR based smFRET to explore the step-wise movement of single aa-tRNAs through ribosomes and to characterize the associated intermediate states.[16, 17] The experimental setup is similar to the one utilized in the studies described in 3.1 and is schematically depicted in Figure 4a. Single ribosomes were bound to 5′-biotinylated mRNAs, initiated with a Cy3 labeled aa-tRNA (fMet-tRNA^{fMet}) in the P site, and immobilized on a microscope slide through biotin–streptavidin interaction. To prevent surface artifacts, the slide had to be passivated beforehand with double stranded DNA and BSA.[17] Cy5 labeled EF-Tu-GTP-aa-tRNA ternary complexes (of Phe-tRNA^{Phe}) were delivered to the tethered ribosomes by stopped-flow. The resulting smFRET time trajectories (Fig. 4b) evolved rapidly from low to high (∼0.75) FRET, followed by dynamic fluctuations to intermediate FRET values (Fig. 4b, cognate). The time (∼93 ms) required to change from low to high FRET is consistent, based on previous studies, with aa-tRNA accommodation.

To dissect the ribosome's reaction pathway, the authors used several reagents that are known to disrupt specific steps. When tetracycline was added, which inhibits aa-tRNA delivery to the A-site,[58] frequent excursions to a 0.35 FRET state as well as occasional excursions to a 0.5 FRET state were observed (Fig. 4b, tetracycline). These events were interpreted as independent attempts of an aa-tRNA to enter the A-site, indicating that tetracycline does not completely disrupt initial binding but rather prevents downstream events in aa-tRNA selection. Next, the non-hydrolysable GTP analogue GDPNP was used to stall the ribosome at the aa-tRNA selection step; the resulting time traces transit rapidly through the 0.35 FRET state and stabilize at the 0.5 FRET state (Fig. 4b, GDPNP), showing that this transition occurs before GTP hydrolysis. Stalling the ribosome after the GTP hydrolysis step with kirromycin, which inhibits the structural change of EF-Tu to the GDP bound conformation,[59, 60] led to fluorescence traces with similar dynamics as those of GDPNP stalled ribosomes (Fig. 4b, kirromycin). Cleavage of a single phosphodiester bond within the sarcin-ricin loop (SRL), a highly conserved region within the 50S subunit, by the plant toxin α-sarcin inhibits EF-Tu mediated tRNA delivery. When ribosomes were cleaved with restrictocin (an α-sarcin analogue) prior to surface immobilization, the resulting time traces showed a rapid transition to a prolonged 0.5 FRET state (Fig. 4b, cleaved SRL), followed by occasional transitions to the 0.75 FRET state. Ribosomes with a cleaved SRL thus took 13-fold longer to reach the 0.75 FRET state than uncleaved ribosomes, and only 15% of the observed aa-tRNAs effectively reached this state.

Finally, the authors investigated fidelity in aa-tRNA selection and proofreading by programming the mRNA at the A-site with a near-cognate codon (CUU instead of the cognate UUU) or a non-cognate one (AAA). The non-cognate codon effectively eliminated aa-tRNA access to the 0.35 FRET state on the time scale of the observations. Time traces with the near-cognate codon showed that the 0.35 FRET state is transiently occupied and, rarely, also the higher FRET states (Fig. 4b, near-cognate). Comparison of cognate and near-cognate smFRET traces allowed the authors to estimate that cognate aa-tRNAs are preferred over near-cognate aa-tRNAs ~6-fold in the initial step and ~24-fold in the second step of proofreading. These findings provide evidence for a kinetic proofreading model with two steps of discrimination against near-cognate aa-tRNAs, one before and one after GTP hydrolysis. Such a mechanism explains how high fidelity can be attained based on relatively small differences in binding free energy between cognate and near-cognate codon–anticodon interactions.

This work exemplifies how smFRET can be used to observe and quantitatively characterize intermediate states of biomolecular machines as large and complex as the ribosome. Many additional applications can easily be envisioned.

4. NUCLEIC ACID NANOTECHNOLOGY

DNA represents a versatile material for building nanostructures because DNA molecules assemble in a very well defined manner (as dictated by Watson-Crick base pairs). Seeman first proposed to use DNA for nanotechnology in 1982,[61] and especially in recent years considerable progress has been made towards this goal.[18, 19] Below we present two examples that markedly illustrate this progress.

4.1. A DNA Based Nanomechanical Device

In nature DNA is mostly found as a right-handed B-form helix. However, a left-handed conformation called Z-DNA is transiently formed when DNA becomes considerably under-wound, for example in the wake of a transcribing RNA polymerase.[62] It has been long recognized that the structural transition between B- and Z-DNA can provide a basis to drive nanomechanical devices,[63] but initial attempts failed owing to the flexibility of its components.[64] Seeman and coworkers overcame this problem by using rigid DNA handles, formed by two DNA double crossover (DX) molecules (Fig. 5a).[18] Their device is composed of a total of three cyclic DNA strands, the two blue ones on the ends, and the red/yellow one in between, as shown in Figure 5a. The central strand links the two DX molecules by a base paired palindromic sequence $d(m^5CG)_{10}$, called a 'proto-Z' sequence (yellow, Fig. 5a), where 5-methylated cytosines, $d(m^5C)$, increase the propensity to undergo the

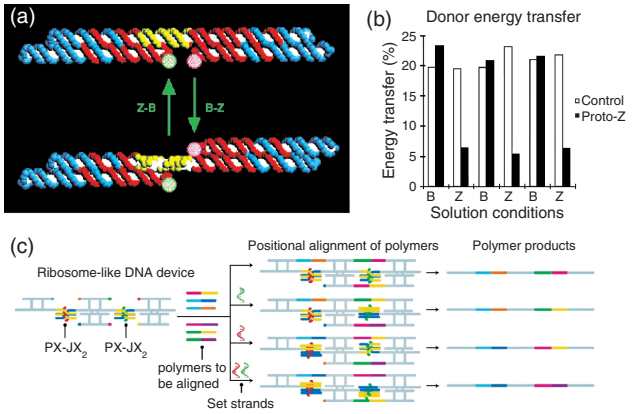

Fig. 5. Nucleic acids in nanotechnology. (a) Design of a nanomechanical device based on the B–Z transition.[1, 18] (b) Changes in energy transfer (FRET) upon changing the solution conditions from promoting B- to Z-DNA and vice versa. (c) A DNA based nanodevice that controls positional polymer assembly.[1, 18] At its heart, two PX-JX[2] molecules can adopt four distinct structural states that enable alignment of six different polymers in four possible ways. The presence or absence of two set strands controls this nanodevice's state. Ligation and purification of the bound polymers gives rise to four programmable products. See text for details. Reproduced with permission from [1], H. Yan, *Science* 306, 2048 **(2004)** and [18], C. Mao et al., *Nature* 397, 144 **(1999)**.

B–Z transition. At high ionic strength this sequence is specifically converted into left-handed Z-DNA, causing a large conformational change with a rotary motion that moves the two ends of the red strand far apart. To follow the conformational transitions between the B- and Z-DNA structures by ensemble FRET, Seeman and coworkers then simply labeled the rotating ends with a donor/acceptor fluorophore pair (Fig. 5a). Figure 5b shows the resulting relative FRET efficiencies upon repeated switching between buffer conditions promoting either B- or Z-DNA.[18] As expected from the schematic in Figure 5a, switching to Z-promoting conditions increases the distance between the fluorophores, resulting in a lower FRET efficiency, while returning to B-DNA promoting conditions reverses this change repeatedly. A non-proto-Z control sequence does not show these changes (Fig. 5b).

This work represented the first demonstration that nanomechanical devices can be constructed using DNA as a raw material. Such a DNA based nanoscale device should be possible to incorporate as a switchable molecular motor into larger assemblies produced by nanotechnology. It is expected to also be capable of moving loads, just as fluorophores were moved in the described work.

4.2. A DNA Device that Synthesizes Programmable DNA Sequences

The chemical composition of a DNA molecule provides precise molecular recognition properties that can be exploited for constructing molecular devices from the bottom-up by assembly in parallel steps.[65] Going a step further, Seeman and coworkers have recently provided

proof-of-principle that DNA nanodevices can be employed to perform useful tasks; they built a self-assembled DNA machine that can control positional polymer synthesis.[19] The machine thus mimics the translational capabilities of the ribosome in that a DNA signal causes the machine to position a series of molecules specifically so that they can be linked together. Importantly, there is no sequence complementarity between the molecules in the assembly line of the "nanofactory" and the manufactured products. At the heart of the DNA device, depicted schematically in Figure 5c, are two PX-JX_2 molecules. PX-JX_2 molecules are made of four DNA strands joined by reciprocal exchange (Fig. 5c).[66] Each PX-JX_2 molecule can adopt two alternate conformations (PX or JX_2) depending on the sequences of two of its strands, judiciously called "set" strands (either green or red in Fig. 5c), such that the DNA device can be prearranged into four distinct conformational states (PX/PX, PX/JX_2, JX_2/PX, and JX_2/JX_2).[19] Each conformational state allows the positioning of two specific DNA motifs (polymers to be aligned, Fig. 5c). These motifs can then be covalently linked together through addition of a ligase enzyme, and the products can be recovered.[19]

This simple prototype clearly demonstrates the feasibility of nanometer scale synthetic machines for nanotechnology. Furthermore, it represents a general encryption device or a finite state machine with variable input as a component of larger programmable DNA-based assemblies.

5. A VISION FOR THE FUTURE: MERGING FIELDS

Traditionally, single molecule fluorescence imaging and nanotechnology have been separate research thrusts, often led by researchers of distinct backgrounds, typically biophysicists and materials engineers, respectively. We envision, however, that the two fields will begin to grow closer and develop many synergies. For example, imagine to be able to monitor in real-time the functional states and precise locations of a spatially distributed network of nanoscale devices—this capability will provide the basis to maintain full control over form and function of the network. How will that be possible? As illustrated in Sections 3 and 4.1, smFRET can monitor the functional state of, for example, a nucleic acid (enzyme). Combine that with (i) the recent demonstration of nanometer-precision localization of single fluorophores by measuring the centroid of their images[67–69] and (ii) the advent of extraordinarily bright, uniformly excitable but multi-colored and photobleaching-resistant fluorophores such as quantum dots[70] and the simultaneous interrogation of both functional state and location of an array of molecular scale devices over long periods of time is possible. In the future, we will thus be able to follow moving nanorobots as they fulfill tasks, detect the delivery of drugs by a miniscule therapeutic vehicle, read out diagnostic and environmental nanosensors in real-time, measure online the production rate of a nanofactory, and watch the self-assembly of a nanomachine.

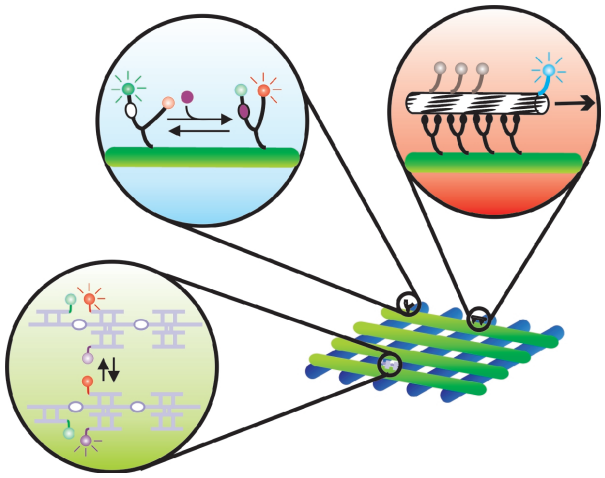

Fig. 6. Vision of future applications of nucleic acid nanotechnology combined with single molecule fluorescence detection. A DNA nanoarray (blue and green rods) is functionalized with multiple nanodevices. Green inset: a DNA-based nanofactory similar to the one described in Section 4.2 changes its conformation to synthesize a programmed product. Three fluorophores (green, red and purple spheres) enable monitoring of this conformational change. The green fluorophore is first excited and, in the initial conformation, the fluorescence from the red fluorophore is observed as a result of FRET. In the final conformation the purple fluorophore is now closer to the donor and its fluorescence is observed. Blue inset: A fluorophore labeled (green and red spheres) RNA nanosensor (black) is attached to the DNA nanoarray (green cylinder). Initially the nanosensor adopts an open conformation so that green fluorescence is observed. Upon binding of the target molecule (purple sphere) the nanosensor adopts a more compact conformation, enabling FRET to the red fluorophore. This specific signal can be used to measure and quantify the presence of the target molecule. Red inset: The DNA nanoarray (green cylinder) functionalized with kinesins (black) carries a molecular shuttle across different regions of the nanoarray. This molecular shuttle can be charged with specific loads (grey spheres). A quantum-dot (blue sphere) attached at the forefront of the molecular shuttle provides a fluorescent signal to monitor and control this transportation nanodevice and its performance.

Figure 6 shows a schematic DNA array based on this vision. Several nanodevices are spatially distributed on the DNA array (insets), for example, a nanofactory similar to the one described in Section 4.2. By employing three-color FRET using one donor and two (different or identical) acceptor fluorophores[71, 72] one could follow in real-time the functional state and productivity of each such nanodevice on the array (green inset of Fig. 6). Furthermore, a nucleic acid based nanosensor could be utilized that changes conformation upon binding of a target molecule. Donor and acceptor fluorophores could be positioned at the extremities of the nanosensor, such that, upon binding of the target molecule, the two fluorophores are brought in close proximity, yielding a target-specific FRET signal (blue inset in Fig. 6). If coupled with a target-dependent enzymatic activity[33] or spring-loaded conformational switch, such a nucleic acid based nanosensor could trigger the release of a molecular shuttle that carries cargo from one location on

the DNA array to another (red inset in Fig. 6). More specifically, quantum-dot labeled, kinesin driven microtubules[2] as depicted in Figure 6 could be used to transport and deliver a new set of reactants to the nanofactory, thereby reprogramming it to make alternate products in response to the target molecule detected by the nanosensor. For inspiration on transportation devices based on biomolecular motors we would like to refer to the recent review by Vogel and coworkers.[2]

While such a multifunctional array has not been assembled yet, each of its components has been demonstrated as feasible. It will only be a matter of time until we begin to see such arrays emerge. FRET and single molecule fluorescence detection will likely be the basis to observe and then control each component separately.

Acknowledgments: This paper is dedicated to Professor Dan Axelrod, who retires this year. His graduate level course on Biophysical Applications of Optical Microscopy at the University of Michigan has been a great inspiration to write this review. The authors would like to thank especially present and former members of the laboratory of NGW for useful comments and discussions. NGW is funded through NIH grant GM62357 and Dow Corning Assistant Professorship and Camille Dreyfus Teacher-Scholar Awards.

References and Notes

1. H. Yan, *Science* 306, 2048 (**2004**).
2. H. Hess, G. D. Bachand, and V. Vogel, *Chemistry* 10, 2110 (**2004**).
3. L. Stryer and R. P. Haugland, *Proc. Natl. Acad. Sci. USA* 58, 719 (**1967**).
4. L. Stryer, *Ann. Rev. Biochem.* 47, 819 (**1978**).
5. N. G. Walter, *Methods* 25, 19 (**2001**).
6. N. G. Walter, D. A. Harris, M. J. Pereira, and D. Rueda, *Biopolymers* 61, 224 (**2001**).
7. F. Kulzer and M. Orrit, *Ann. Rev. Phys. Chem.* 55, 585 (**2004**).
8. S. Weiss, *Science* 283, 1676 (**1999**).
9. S. Weiss, *Nat. Struct. Biol.* 7, 724 (**2000**).
10. T. Ha, *Methods* 25, 78 (**2001**).
11. X. Michalet, A. N. Kapanidis, T. Laurence, F. Pinaud, S. Doose, M. Pflughoefft, and S. Weiss, *Annu. Rev. Biophys. Biomol. Struct.* 32, 161 (**2003**).
12. E. A. Jares-Erijman and T. M. Jovin, *Nat. Biotechnol.* 21, 1387 (**2003**).
13. X. Zhuang, *Ann. Rev. Biophys. Biomol. Struct.* (**2004**).
14. G. Bokinsky, D. Rueda, V. K. Misra, M. M. Rhodes, A. Gordus, H. P. Babcock, N. G. Walter, and X. Zhuang, *Proc. Natl. Acad. Sci. USA* 100, 9302 (**2003**).
15. X. Zhuang, H. Kim, M. J. Pereira, H. P. Babcock, N. G. Walter, and S. Chu, *Science* 296, 1473 (**2002**).
16. S. C. Blanchard, R. L. Gonzalez, H. D. Kim, S. Chu, and J. D. Puglisi, *Nat. Struct. Mol. Biol.* 11, 1008 (**2004**).
17. S. C. Blanchard, H. D. Kim, R. L. Gonzalez, Jr., J. D. Puglisi, and S. Chu, *Proc. Natl. Acad. Sci. USA* 101, 12893 (**2004**).
18. C. Mao, W. Sun, Z. Shen, and N. C. Seeman, *Nature* 397, 144 (**1999**).
19. S. Liao and N. C. Seeman, *Science* 306, 2072 (**2004**).
20. N. C. Seeman, *Nature* 421, 427 (**2003**).
21. N. C. Seeman, *Chem. Biol.* 10, 1151 (**2003**).
22. T. Forster, *Annal. Physik* 2, 55 (**1948**).
23. A. A. Deniz, T. A. Laurence, M. Dahan, D. S. Chemla, P. G. Schultz, and S. Weiss, *Ann Rev. Phys. Chem.* 52, 233 (**2001**).
24. G. Pljevaljcic, D. P. Millar, and A. A. Deniz, *Biophys. J.* 87, 457 (**2004**).
25. H. P. Lu, L. Xun, and X. S. Xie, *Science* 282, 1877 (**1998**).
26. T. Ha, X. Zhuang, H. D. Kim, J. W. Orr, J. R. Williamson, and S. Chu, *Proc. Natl. Acad. Sci. USA* 96, 9077 (**1999**).
27. W. R. Zipfel, R. M. Williams, and W. W. Webb, *Nat. Biotechnol.* 21, 1369 (**2003**).
28. D. Axelrod, T. P. Burghardt, and N. L. Thompson, *Ann Rev. Biophys. Bioeng.* 13, 247 (**1984**).
29. B. A. Sullenger and E. Gilboa, *Nature* 418, 252 (**2002**).
30. R. R. Breaker, *Nature* 432, 838 (**2004**).
31. G. J. Hannon and J. J. Rossi, *Nature* 431, 371 (**2004**).
32. J. Silva, K. Chang, G. J. Hannon, and F. V. Rivas, *Oncogene* 23, 8401 (**2004**).
33. P. T. Sekella, D. Rueda, and N. G. Walter, *RNA* 8, 1242 (**2002**).
34. R. R. Breaker, *Curr. Opin. Biotechnol.* 13, 31 (**2002**).
35. A. Chworos, I. Severcan, A. Y. Koyfman, P. Weinkam, E. Oroudjev, H. G. Hansma, and L. Jaeger, *Science* 306, 2068 (**2004**).
36. W. C. Winkler, A. Nahvi, A. Roth, J. A. Collins, and R. R. Breaker, *Nature* 428, 281 (**2004**).
37. S. Valadkhan and J. L. Manley, *Nature* 413, 701 (**2001**).
38. T. Villa, J. A. Pleiss, and C. Guthrie, *Cell* 109, 149 (**2002**).
39. P. B. Moore and T. A. Steitz, *Nature* 418, 229 (**2002**).
40. V. Ramakrishnan, *Cell* 108, 557 (**2002**).
41. R. H. Symons, *Nucleic Acids Res.* 25, 2683 (**1997**).
42. J. A. Doudna and T. R. Cech, *Nature* 418, 222 (**2002**).
43. R. H. Symons, *Ann Rev. Biochem.* 61, 641 (**1992**).
44. P. B. Rupert and A. R. Ferre-D'Amare, *Nature* 410, 780 (**2001**).
45. Z. Cai and I. Tinoco, Jr., *Biochemistry* 35, 6026 (**1996**).
46. S. E. Butcher, F. H. Allain, and J. Feigon, *Nat. Struct. Biol.* 6, 212 (**1999**).
47. P. B. Rupert, A. P. Massey, S. T. Sigurdsson, and A. R. Ferre-D'Amare, *Science* 298, 1421 (**2002**).
48. X. Zhuang, L. E. Bartley, H. P. Babcock, R. Russell, T. Ha, D. Herschlag, and S. Chu, *Science* 288, 2048 (**2000**).
49. M. Mrksich and G. M. Whitesides, *Ann. Rev. Biophys. Biomol. Struct.* 25, 55 (**1996**).
50. T. Ha, I. Rasnik, W. Cheng, H. P. Babcock, G. H. Gauss, T. M. Lohman, and S. Chu, *Nature* 419, 638 (**2002**).
51. D. Rueda, G. Bokinsky, M. M. Rhodes, M. J. Rust, X. Zhuang, and N. G. Walter, *Proc. Natl. Acad. Sci. USA* 101, 10066 (**2004**).
52. S. J. Benkovic and S. Hammes-Schiffer, *Science* 301, 1196 (**2003**).
53. A. R. Fersht, A. Matouschek, and L. Serrano, *J. Mol. Biol.* 224, 771 (**1992**).
54. K. B. Gromadski and M. V. Rodnina, *Mol. Cell* 13, 191 (**2004**).
55. M. V. Rodnina, K. B. Gromadski, U. Kothe, and H. J. Wieden, *FEBS Lett.* 579, 938 (**2005**).
56. J. Parker, *Microbiol. Rev.* 53, 273 (**1989**).
57. A. Sytnik, S. Vladimirov, Y. Jia, L. Li, B. S. Cooperman, and R. M. Hochstrasser, *J. Mol. Biol.* 285, 49 (**1999**).
58. E. Cundliffe, in *Ribosome, Structure, Function, and Genetics. Proceedings of the 9th Steenbock Symposium,* edited by G. Chambliss, University Park Press, Baltimore (**1979**), p. 555.
59. H. Wolf, G. Chinali, and A. Parmeggiani, *Eur. J. Biochem.* 75, 67 (**1977**).
60. L. Vogeley, G. J. Palm, J. R. Mesters, and R. Hilgenfeld, *J. Biol. Chem.* 276, 17149 (**2001**).
61. N. C. Seeman, *J. Theor. Biol.* 99, 237 (**1982**).
62. T. Schwartz, M. A. Rould, K. Lowenhaupt, A. Herbert, and A. Rich, *Science* 284, 1841 (**1999**).
63. N. C. Seeman, in *Biomolecular Materials*, edited by C. Viney, S. T. Case, and J. H. Waite, Materials Research Soc., Pittsburgh, PA (**1993**), Vol. 292, p. 123.
64. R. I. Ma, N. R. Kallenbach, R. D. Sheardy, M. L. Petrillo, and N. C. Seeman, *Nucleic Acids Res.* 14, 9745 (**1986**).

65. N. C. Seeman and A. M. Belcher, *Proc. Natl. Acad. Sci. USA* 99, 6451 **(2002)**.
66. H. Yan, X. Zhang, Z. Shen, and N. C. Seeman, *Nature* 415, 62 **(2002)**.
67. R. E. Thompson, D. R. Larson, and W. W. Webb, *Biophys. J.* 82, 2775 **(2002)**.
68. A. Yildiz, J. N. Forkey, S. A. McKinney, T. Ha, Y. E. Goldman, and P. R. Selvin, *Science* 300, 2061 **(2003)**.
69. A. Yildiz, M. Tomishige, R. D. Vale, and P. R. Selvin, *Science* 303, 676 **(2004)**.
70. X. Michalet, F. F. Pinaud, L. A. Bentolila, J. M. Tsay, S. Doose, J. J. Li, G. Sundaresan, A. M. Wu, S. S. Gambhir, and S. Weiss, *Science* 307, 538 **(2005)**.
71. J. P. Clamme and A. A. Deniz, *Chem. Phys. Chem.* 6, 74 **(2005)**.
72. S. Hohng, C. Joo, and T. Ha, *Biophys. J.* 87, 1328 **(2004)**.

Received: 7 April 2004. Revised/Accepted: 5 May 2005.